arXiv:astro-ph/0208107v1 6 Aug 2002

OBSERVATION OF MULTI-TeV DIFFUSE GAMMA RAYS FROM THE GALACTIC PLANE WITH THE TIBET AIR SHOWER ARRAY

M. Amenomori[1], S. Ayabe[2], S.H. Cui[3], L.K. Ding[3], X.H. Ding[4], C.F. Feng[5] C.Y. Feng[6], Y. Fu[5], X.Y. Gao[7], Q.X. Geng[7], H.W. Guo[4], M. He[5], K. Hibino[8], N. Hotta[9], J. Huang[9], Q. Huang[6], A.X. Huo[3], K. Izu[10], H.Y. Jia[6], F. Kajino[11], K. Kasahara[12], Y. Katayose[13], K. Kawata[11], Labaciren[4], G.M. Le[14], J.Y. Li[5], H. Lu[3], S.L. Lu[3], G.X. Luo[3], X.R. Meng[4], K. Mizutani[2], J. Mu[7], H. Nanjo[1], M. Nishizawa[15], M. Ohnishi[10], I. Ohta[9], H. Ooura[11], T. Ouchi[10], S. Ozawa[9], J.R. Ren[3], T. Saito[16], M. Sakata[11], T. Sasaki[8], M. Shibata[13], A. Shiomi[10], T. Shirai[8], H. Sugimoto[17], K. Taira[17], M. Takita[10], Y.H. Tan[3], N. Tateyama[8], S. Torii[8], H. Tsuchiya[10], S. Udo[2], T. Utsugi[2], C.R. Wang[5], H. Wang[3], X. Wang[5], X.W. Xu[3], L. Xue[5], X.C. Yang[7], Y. Yamamoto[11], Z.H. Ye[14], G.C. Yu[6], A.F. Yuan[4], T. Yuda[18], H.M. Zhang[3], J.L. Zhang[3], N.J. Zhang[5], X.Y. Zhang[5], Zhaxiciren[4] and Zhaxisangzhu[4]
(The Tibet ASγ Collaboration)

ABSTRACT

Data from the Tibet-III air shower array (with energies around 3 TeV) and from the Tibet-II array (with energies around 10 TeV) have been searched for diffuse gamma rays from the Galactic plane. These arrays have an angular resolution of about 0.9 degrees. The sky regions searched are the inner Galaxy, $20^\circ \leq l \leq 55^\circ$, and outer Galaxy, $140^\circ \leq l \leq 225^\circ$, and $|b| \leq 2^\circ$ or $\leq 5^\circ$. No significant Galactic plane gamma-ray excess was observed. The 99% confidence level upper limits for gamma-ray intensity obtained are (for $|b| \leq 2^\circ$) 1.1×10^{-15} $\mathrm{cm^{-2}s^{-1}sr^{-1}MeV^{-1}}$ at 3 TeV and 4.1×10^{-17} $\mathrm{cm^{-2}s^{-1}sr^{-1}MeV^{-1}}$ at 10 TeV for the inner Galaxy, and 3.6×10^{-16} $\mathrm{cm^{-2}s^{-1}sr^{-1}MeV^{-1}}$ at 3 TeV and 1.3×10^{-17} $\mathrm{cm^{-2}s^{-1}sr^{-1}MeV^{-1}}$ at 10 TeV for the outer Galaxy, assuming a differential spectral index of 2.4. The upper limits are significant in the multi-TeV region when compared to those from Cherenkov telescopes in the lower energy region

[1] Department of Physics, Hirosaki University, Hirosaki 036-8561, Japan

[2] Department of Physics, Saitama University, Saitama 338-8570, Japan

[3] Laboratory of Cosmic Ray and High Energy Astrophysics, Institute of High Energy Physics, Chinese Academy of Sciences, Beijing 100039, China

[4] Department of Mathematics and Physics, Tibet University, Lhasa 850000, China

[5] Department of Physics, Shangdong University, Jinan 250100, China

[6] Institute of Modern Physics, South West Jiaotong University, Chengdu 610031, Chi na

[7] Department of Physics, Yunnan University, Kunming 650091, China

[8] Faculty of Engineering, Kanagawa University, Yokohama 221-8686, Japan

[9] Faculty of Education, Utsunomiya University, Utsunomiya 321-8505, Japan

[10] Institute for Cosmic Ray Research, University of Tokyo, Kashiwa 277-8582, Japan

[11] Department of Physics, Konan University, Kobe 658-8501, Japan

[12] Faculty of Systems Engineering, Shibaura Institute of Technology, Saitama 330-8570, Japan

[13] Faculty of Engineering, Yokohama National University, Yokohama 240-0067, Japan

[14] Center of Space Science and Application Research, Chinese Academy of Sciences, B eijing 100080, China

[15] National Institute for Informatics, Tokyo 112-8640, Japan

[16] Tokyo Metropolitan College of Aeronautical Engineering, Tokyo 116-0003, Japan

[17] Shonan Institute of Technology, Fujisawa 251-8511, Japan

[18] Solar-Terrestrial Environment Laboratory, Nagoya University, Nagoya 464-8601, Japan

and other air shower arrays in the higher energy region; however, the results are not sufficient to rule out the inverse Compton model with a source electron spectral index of 2.0.

Subject headings: cosmic rays—Galactic plane—diffuse gamma rays: observations

1. INTRODUCTION

Detection of diffuse gamma rays from the Galactic plane is considered to be a promising way to understand spatial distributions of cosmic-ray acceleration regions, of interstellar matter (ISM), and interstellar photon field (ISPF) densities. Experimental data in the energy region below 10 GeV with the EGRET instrument Hunter et al. 1997, are fairly well interpreted in terms of interactions of cosmic-ray hadrons and electrons with ISM and ISPF. However, a portion of the contribution of each elementary process of interaction is uncertain due to assumed intensities and spectral indices of cosmic-ray hadrons, electrons, and densities of ISM and ISPF. With experiments in the energy region above 100 GeV, only upper limits for diffuse gamma-ray intensities have been obtained, and these results provide some constraints on the parameters in the models. In order to constrain the parameter values more severely in this energy region, it is necessary to obtain more observational data.

In the early stage of cosmic-ray astrophysics, the production rate of gamma rays by Compton scattering of starlight photons by cosmic-ray electrons was calculated by Feenberg & Primakoff (1948), and gamma rays arising from neutral pions through cosmic-ray collision with ISM was studied by Hayakawa (1952). Morrison (1958) advocated gamma-ray astronomy because of the known production mechanisms and the straight trajectories from the origin. Ginzburg & Syrovatskii (1964) summarized the elementary process for gamma-ray production and discussed diffusion and propagation of cosmic rays in the Galactic disc. As a result, it is quite natural to expect gamma rays from the Galactic plane, however was twenty years after the pioneering work by Feenberg & Primakoff (1948) until the intense band of gamma-ray intensity along the Galactic plane was observed with OSO 3 Kraushaar et al. 1972 and a balloon-borne detector Fichtel et al. 1972. Advanced observations were carried out by detectors borne on SAS 2 (Fichtel et al. 1975; Hartman et al. 1979) and COS B (Mayer-Hasselwander et al. 1980, 1982). These observations revealed that the intensity profile of high-energy gamma rays is quite relevant to the structure of the Galaxy, and have stimulated much theoretical work in gamma-ray astronomy below 10 GeV (see, Bertsch et al. 1993 and references therein).

A detailed intensity distribution of high-energy gamma rays coming from the Galactic plane was given by Hunter et al. (1997) based on EGRET observations. In the energy region above 1 GeV, the gamma-ray intensity from the inner Galaxy is higher than the COS B data by a factor of about 3. It is also higher than the conventional model predictions (e.g., Hunter et al. 1997; Bertsch et al. 1993) by a factor of 1.7, where the neutral pion production is based on the calculations of Stecker (1988), assuming the power law proton spectrum with spectral index of 2.75 Dermer 1986. Mori (1997) showed that the latter discrepancy can not be attributed to a calculation with inaccurate accelerator data on neutral pion production. It can, however, be interpreted by adopting a harder proton spectral index of 2.45 for the EGRET excess within a plane thickness of $|b| \leq 10^{\circ}$. Webber (1999) also showed that the EGRET excess in $|b| \leq 5^{\circ}$ can be reproduced by assuming a source proton spectral index of 2.25.

Following an indication by Schlickeiser (1979) of the importance of using the Klein-Nishina cross section, Protheroe & Wolfendale (1980) showed possible dominance of inverse Compton (IC) gamma rays over neutral-pion decay gamma rays for a range of electron injection spectra. Detailed calculations of IC gamma rays above 50 MeV were made by Chi et al. (1989), which were more than 50 % of the total diffuse intensity at a medium galactic latitude of $|b| = 10^{\circ} - 20^{\circ}$. Porter & Protheroe (1997) indicated that in such a high-energy region, cosmic-ray electrons may create a significant part of the diffuse gamma rays, depending on their injection spectral index and acceleration cutoff energy. Pohl & Esposito (1998) remarked that most of radio synchrotron spectra of SNRs are well represented by power law indices around 0.5, corresponding to an electron injection index of about 2.0 Green 1995. They argued that if this injection electron index is employed, the EGRET excess above 1 GeV can be well explained by IC scattering. They also argued that an electron injection index of 2.0 is within the expected Poisson fluctuations and is reasonable in the direction toward the Galactic center with the line of sight passing through the vicinity of many SNRs, taking into account the diffusion coefficient and the observed local electron index of around 3.0 below 1 TeV. Recently, the energy spectrum of local electrons has been obtained with balloon-borne instruments HEAT Barwick et al. 1998 and BETS Torii et al. 2001.

Some models of diffuse Galactic gamma-ray continuum radiation below 10 GeV were synthetically discussed by Strong, Moskalenko, & Reimer (2000) with respect to the injection spectra, including a harder nucleon and electron spectral indices, and also with respect to different ISM and ISPF densities. At the higher energies of the TeV-PeV region, the diffuse gamma-ray emission was calculated by Berezinsky et al. (1993) in terms of cosmic-ray interaction with ISM, and also by Ingelman & Thunman (1996) using the current models for high energy particle interaction. Broad-band diffuse gamma-ray

emission, covering the MeV-PeV region, was comprehensively calculated by Aharonian & Atoyan (2001), and they discussed propagation of hadron and electron components and their injection spectra. Assuming that the hadron spectral index is 2.15 (or 2.0) in SNRs, Berezhko & Völk (2000) showed that the averaged contribution to the diffuse gamma-ray flux should exceed the current model predictions (Hunter et al. 1997; Bertsch et al 1993) by a factor 5 (or 29) at 1 TeV.

Recently, several groups gave upper limits for diffuse gamma-ray fluxes (Borione et al. 1998) above 100 TeV from the outer Galactic plane, using large ground-based air shower arrays and muon detectors, and above 500 GeV LeBohec et al. 2000 and around 1 TeV Aharonian et al. 2001 from the inner Galactic plane, using imaging atmospheric Cherenkov telescopes (IACT). Using a small scintillation counter array, Tibet-I, upper limits Amenomori et al. 1997 were given at 10 TeV from the inner and outer Galactic planes. In this paper we report new upper limits from both the enlarged Tibet-II array and the high detector density array of Tibet-III.

2. EXPERIMENT

After three years of operation, starting in 1990, of the Tibet-I array (located at an altitude of 4300 m a.s.l. (606 gcm^{-2}) at Yangbajing (90.53°E, 30.11°N) in Tibet of China), many scintillation counters were added to this array late in 1994 to improve the sensitivity to allow detection of ∼10 TeV gamma rays from a known source like the Crab Nebula, and from other possible sources as well. The Tibet-II array consists of 221 scintillation counters of 0.5 m^2 each, keeping the same lattice interval of 15 m as Tibet-I. The performance of the Tibet-II array is almost same as the Tibet-I which is described elsewhere (Amenomori et al. 1992, 1993). The mode energy of all triggered air showers is estimated from simulations to be about 7 TeV and 8 TeV for proton initiated showers with a spectral index of 2.7 and gamma-ray initiated ones assuming a spectral index of 2.5, respectively. The mode energy is 10 TeV for air showers with $\Sigma\rho_{\rm FT} \geq 15$ m^{-2}, where $\Sigma\rho_{\rm FT}/2$ is the sum of the number of particles that hit all 0.5 m^2 detectors. This mode energy can be calibrated by the magnitude of the westward shift of the moon shadow, and the maximum deficit position due to the geomagnetic effect (Amenomori et al. 1993, 1996). The angular resolution is determined to be 0.9° at 10 TeV, also using the deficit shape (depth and width) of the moon shadow.

The Tibet-II array covers 36,900 m^2, which is 4.5 times larger than Tibet-I, except for some scattered detectors surrounding the lattice area in each array Amenomori et al. 1995 as shown in Fig. 1. The data acquisition rate is about 200 Hz with the trigger condition requiring any four detectors to have 0.80 particles per detector. The observed number of

air showers is 5.44 $\times 10^9$ events after the pre-analysis determining the arrival direction and shower axis location, for the effective 551.2 days during the period 1997 February through 1999 September. The event rate is about 114 events per second in the Tibet-II data.

In 1999, the array was enlarged, with many more scintillation counters so as to make a high detector density array, Tibet-III, with a 7.5 m lattice interval. Fig. 1 shows the status in 2001. The Tibet-III array consists of 533 scintillation counters covering 22,050 m^2. The full Tibet-III array will be completed in 2002; it will cover 36,900 m^2, the same as Tibet-II, as described in Amenomori et al. (2001). The mode energy of Tibet-III is about 3 TeV for proton initiated showers and the angular resolution is 0.87° in the energy region above 3 TeV. The data acquisition rate is 680 Hz with the same trigger condition as described above for Tibet-II. The number of air showers is 1.35 $\times 10^{10}$ events, of which the arrival direction and shower axis location are determined for the effective 517.3 days during the period 1999 November through 2001 October. The event rate is about 302 events per second in the Tibet-III data. The performance of these arrays and the data obtained are summarized in Table 1.

TABLE 1
ARRAY PERFORMANCE AND OBTAINED DATA

Air Shower Array	Lattice Interval (m)	Inner Area (m^2)	Trigg Rate† (Hz)	Observd Period Net days	Pre-analysis for $\Sigma\rho_{\rm FT} \geq 15$ Events (10^9)	$E_{\rm mode}$ (TeV)	Ang. res. (deg.)	Inner Events (10^9)
Tibet-II	15	28,350	200	1997 Feb ∼99 Sep 551.2	5.44	10	0.9	4.14
Tibet-III	7.5	22,050*	680	1999 Nov ∼01 Oct 517.3	13.5	3	0.87	6.59

† Trigger level is any four detectors with 0.80 particles per detector.

* At the status in 1999∼2002. The inner area is increased to ∼32,500 m^2 till the end of 2002.

Figure 2 shows an exposure map in galactic coordinates for air showers obtained with the Tibet-III array, with zenith angles $\theta \leq 50°$. The shower event density increases from light gray to dark gray. The Tibet-II array data produce a quite similar map. For the on-plane data, shower events are employed in the sky regions of $20° \leq l \leq 55°$ for the inner Galaxy (IG) and of $140° \leq l \leq 225°$ for the outer Galaxy (OG), in $|b| \leq 2°$ or $\leq 5°$ along the Galactic plane.

3. DATA ANALYSIS

For the analysis in the energy range around 10 TeV, 4.14 $\times 10^9$ air shower events are used with zenith angles $\theta \leq 50^\circ$, whose axes hit the inner area of 28,350 m^2 of the Tibet-II array to assure the quality of the arrival angle determination. Around 3 TeV, 6.59 $\times 10^9$ events are used with $\theta \leq 50^\circ$ whose axes hit the 7.5 m lattice area of 22,050 m^2 of the Tibet-III array. The number of events that hit these inner areas are tabulated also in Table 1 in the last column. Those air shower events are assigned to the sky regions from which they arrived, of $4^\circ(10^\circ)$ bin 90 (36) belts along the Galactic plane in equatorial coordinates both for the Tibet-II and Tibet-III array data. Figure 3 shows 10° bin warped belts for IG with the declination range of $-10^\circ \leq \delta \leq 20^\circ$ and OG with $-10^\circ \leq \delta \leq 60^\circ$. These declination ranges of the on-plane belts in the equatorial coordinates correspond to parts of a convex lens shape, with a maximum thickness of about 4° or 10° in galactic coordinates, as shown in Fig. 2. The primary reason those warped belts are employed is to detect gamma-ray signals as accurately as possible if they are emitted from the Galactic plane with greater intensity than from other sky regions. In addition, the zenith angle distribution, and hence the primary energies of detected air showers are quite similar in each warped belt. This is very important doing the estimation of the on-plane background intensity at the same energy for both the on-plane and many off-plane belts, because the gamma-ray energy spectrum is still unknown. The final reason is that the background estimate, especially for the OG, is little affected by the IG plane, because the warped belts crossing the IG plane do so diagonally, over a narrow band of longitudes.

Figure 4 shows the distribution of the number of events in 4° bin warped belts. The abscissa represents the right ascension of each warped belt at the declination 30°, which is the same as the latitude of the Yangbajing site. The solid lines are the curves fitted to the experimental data, ignoring the on-plane data. In this figure, the cases for (a) IG and (b) OG in the Tibet-III data at 3 TeV and (c) IG and (d) OG in the Tibet-II data at 10 TeV are shown in the 4° bin analysis. The anisotropy of cosmic-ray intensity seen in this figure, with an amplitude of less than $\pm 1\%$, is mainly due to some seasonal long suspensions of operation for construction and system calibration of the array, and partly due to weather conditions and a slight, 1° or less, inclination of the site at Yangbajing.

An excess of the on-plane data above the fitted curve would be considered to be a gamma-ray signal. The signal strength is measured by a standard deviation of the number of showers, in two or five 2° bin belts, by the formula $(E - B)/\sqrt{B}$, where E is the number of on-plane events and B is the estimated number of background events in the on-plane region. B is estimated from the solid curve which is obtained by the fitting of many 2° bin off-plane belts, ignoring the central 16° or 14° widths corresponding to the 4° bin or 10° bin

belt analyses. We intend to deduce the number of on-plane background events as accurately as possible from this fitting curve of the off-plane data. The number of events shown by the solid curve in each subfigure of Fig. 4 is assumed to be due to galactic cosmic rays. In this method, an isotropic extragalactic diffuse gamma-ray component can not be distinguished from the galactic cosmic rays. We assume that the intensity of the isotropic component is negligible in comparison with the diffuse gamma rays from the Galactic plane.

Figure 5 shows the deviation distributions of the number of events from the fitted curves (the solid ones in Fig. 4) in 2° bin off-plane belts for (a) IG and (b) OG in the Tibet-III data at 3 TeV and (c) IG and (d) OG in the Tibet-II data at 10 TeV, respectively, in the case of the 4° bin analysis. Here, the abscissa represents a significance in the 2° bin off-plane belts. The solid curves are best-fit Gaussians with standard deviations of 0.998, 1.007, 0.999 and 1.000, respectively, and where data on the 12° width centered at the Galactic plane are excluded. In the case of the 10° bin analysis, almost the same distributions are obtained; their standard deviations are 1.018, 1.007, 1.013 and 1.000, respectively. Because the fluctuation of the number of events around the fitted curve in the off-plane belts is quite natural, i.e. each standard deviation is almost equal in unity, the solid curves are considered to be satisfactorily fitted to the experimental data. Thus, we can accurately estimate the number of on-plane background events.

The diffuse gamma-ray intensity from the OG plane is likely to be much lower than that from the IG plane. The well known gamma-ray point source, the Crab Nebula, is located at $\alpha = 83.^{\circ}38', \delta = 22.^{\circ}01'$ ($l = 184.56°, b = -5.78°$) with a real angle distance of 5.78° from the central sheet of the OG plane. The Crab is in the off-plane belt adjacent to the on-plane belt in the 10° bin analysis. In the 4° bin analysis, the Crab is located between the on-plane and off-plane regions but nearer to the latter. For that reason, we omit the two 2° bin warped belts from the off-plane region. As a result, the data in the 8 warped belts, $-10° < b < 6°$, are excluded from the background estimation in the 4° bin analysis, while the 7 warped belts, $-9° < b < 5°$, are excluded in the 10° bin analysis. Thus, the real angle distance of the Crab is 4.21° from the on-plane region and 2.22° from the newly defined off-plane region in the 4° bin analysis, and 1.82° and 1.40° in the 10° bin analysis. Therefore, the Crab is located sufficiently far from both the on-plane and off-plane regions, because the angular resolutions of the Tibet-III at 3 TeV and the Tibet-II at 10 TeV are both about 0.9°.

In order to see the adequacy of the fitting and on-plane excess in more detail, smaller ranges of the right ascension band of about 50° around the Galactic plane are shown in Fig. 6, where subfigures (a), (b), (c) and (d) correspond to those in Fig. 4. In each subfigure, the on-plane and off-plane data are indicated by filled circles and filled triangles, respectively,

and the blank squares indicate the data points excluded from the background estimation. Error bars are statistical only. It is noted that the error bars are short in the subfigure (b) because the ordinate scale is compressed by about half compared to the other subfigures.

4. RESULTS and DISCUSSION

The significance of an on-plane excess, $(E-B)/\sqrt{B}$ measured in standard deviation of the number of on-plane events, is calculated for each distribution shown in Fig. 6 and the results are summarized in Table 2. In Table 2, the results thus obtained are given for the regions of IG ($20^\circ \leq l \leq 55^\circ$) and OG ($140^\circ \leq l \leq 225^\circ$). Mode energies 3 TeV and 10 TeV indicate the analyses of the Tibet-III and Tibet-II data, respectively. As given in this table, no significant excess is found, although an excess of $+2.52\ \sigma$ is marginal for IG at 3 TeV in the 4° bin analysis of the Tibet-III data. We calculate the upper limits for the gamma-ray intensity using the methods given by Helene (1983) and Protheroe (1984), specifically for a small excess or deficit on the Galactic plane. In this table, $J_\gamma/J_{\rm CR}$ means the flux ratio at 1 σ excess, which is identical to $1/\sqrt{B}$, of the diffuse gamma rays versus the galactic cosmic rays in the energy region above 3 TeV and above 10 TeV. A minor component of the isotropic diffuse gamma rays is included in the galactic cosmic rays because separating them is impossible in the Tibet air shower array due to the lack of any equipment to reduce the background hadron initiated air showers.

TABLE 2
LIMITS TO DIFFUSE GAMMA RAYS

Inner or Outer Galactic Plane (Region of l)	Region of b	Mode Energy (TeV)	Significance (σ)	$\frac{J_\gamma(>E)}{J_{\rm CR}(>E)}$ at 1σ ($\equiv 1/\sqrt{B}$) (10^{-4})	$E^2\frac{dJ_\gamma(>E)}{dE}$ ($\rm cm^{-2}s^{-1}sr^{-1}MeV$) 90% CL ($10^{-3}$)	99% CL (10^{-3})
I G ($20^\circ \leq l \leq 55^\circ$)	$\lvert b\rvert < 2^\circ$	3	+2.52	1.95	7.6	9.6
		10	+1.71	2.43	3.0	4.0
	$\lvert b\rvert < 5^\circ$	3	+1.88	1.23	4.0	5.3
		10	+0.81	1.54	1.4	2.0
O G ($140^\circ \leq l \leq 225^\circ$)	$\lvert b\rvert < 2^\circ$	3	+0.25	1.16	2.1	3.3
		10	−0.63	1.45	0.78	1.3
	$\lvert b\rvert < 5^\circ$	3	+1.78	0.737	2.3	3.1
		10	−0.66	0.936	0.50	0.83

In Table 2, the intensity upper limits are also given as 90% and 99% confidence level (CL), calculated from the above flux ratio and assuming a differential spectral index of 2.4

for the diffuse gamma rays, and utlizing the all-particle energy spectrum of the galactic cosmic rays recently compiled by Apanasenko et al. (2001).

Figure 7 shows the 99% CL upper limits thus obtained for diffuse gamma rays from the inner Galactic plane, $20^\circ \leq l \leq 55^\circ$ and $|b| \leq 2^\circ$, at energies around 3 TeV (T3 for Tibet-III) and 10 TeV (T2 for Tibet-II). In this figure the EGRET data Hunter et al. 1997, $315^\circ \leq l \leq 45^\circ$ and $|b| \leq 2^\circ$, are plotted. The Cherenkov data are also plotted, including Whipple's 99.9% CL upper limit above 500 GeV LeBohec et al. 2000 at the region of $38.5^\circ \leq l \leq 41.5^\circ$ and $|b| \leq 2^\circ$, and HEGRA-IACT's 99% CL upper limit above 1 TeV Aharonian et al. 2001 in a similar region of $38^\circ \leq l \leq 43^\circ$ and $|b| \leq 2^\circ$. The theoretical curve calculated by Berezinsky et al. (1993) for $\pi^\circ \rightarrow 2\gamma$ due to the collision of cosmic-ray hadrons with ISM is drawn by a solid curve (BGHS) which is for the region of $20^\circ \leq l \leq 55^\circ$ and $|b| \leq 2^\circ$, deduced from their original paper which is based on the matter density distribution compiled by Fichtel & Kniffen (1984) and Bloemen et al. (1984).

For inverse Compton gamma rays induced by energetic electrons, the calculation by Porter & Protheroe (1996) is shown by dashed curves for source electron spectral indices of 2.0 (PP2.0) and 2.4 (PP2.4) in the direction $l = 0^\circ$ and $b = 0^\circ$, the Galactic center. Similar theoretical curves calculated by Tateyama & Nishimura (2001) are shown by dot-dashed lines with source spectral indices of 2.0 (TN2.0) and 2.4 (TN2.4) in the direction $l = 0^\circ$ and $|b| \leq 2^\circ$. The density distribution of ISPF in their calculations is based on the compilations by Bloemen (1985) and Mathis et al. (1983). The curves from Tateyama & Nishimura (2001) are consistent with the estimations by Porter & Protheroe (1996) considering the different region of $|b|$. The present Tibet data, especially at 10 TeV, together with the HEGRA-IACT data, give the most stringent upper limit for the IC model, although these data can not clearly rule out the IC model with a source electron spectral index of 2.0.

Figure 8 shows the present results as 99% CL upper limits (upper bars of T3 and T2) for diffuse gamma rays from the outer part of the Galactic plane, $140^\circ \leq l \leq 225^\circ$ and $|b| \leq 2^\circ$, for the energy ranges around 3 TeV (T3 for Tibet-III) and 10 TeV (T2 for Tibet-II). In this figure, the 90% CL upper limits (lower bars) are compared with the CASA-MIA 90% CL upper limits, which are based upon muon-poor air showers Borione et al. 1998 at about 140 TeV-1.3 PeV, from the OG plane of $50^\circ \leq l \leq 200^\circ$ and $|b| \leq 2^\circ$. The CASA-MIA data can rule out the IC model with index 2.0 without acceleration energy cutoff, but can not rule out the case with an energy cutoff at 100 TeV. In this figure, the theoretical curve by Berezinsky et al. (1993) is also shown for $\pi^\circ \rightarrow 2\gamma$ component (BGHS) in the region of $140^\circ \leq l \leq 225^\circ$ and $|b| \leq 2^\circ$. The IC gamma rays calculated by Porter & Protheroe (1996) for the region $50^\circ \leq l \leq 200^\circ$ and $|b| \leq 10^\circ$ for source spectral indices of 2.0 (PP2.0) and 2.4 (PP2.4) are shown, as well as the ones by Tateyama & Nishimura

(2001) in the region of $l = 180^\circ$ and $|b| \leq 2^\circ$ for source spectral indices of 2.0 (TN2.0) and 2.4 (TN2.4). The present data are also not sufficient to rule out the IC model with a spectral index of 2.0.

Next we discuss some considerations regarding our method of data analysis and its results. First, a difference of the average shower size between gamma-ray and proton initiated showers with the same energy at the Yangbajing site (606 gcm^{-2}) will produce different initial proton and gamma-ray energies for the same observed shower size. By employing the subroutine package GENAS of Kasahara & Torii (1991), the average incident gamma-ray energy is roughly estimated to be lower by 18% at 3 TeV and lower by 23% at 10 TeV than that for protons of the same shower size, taking the median zenith angle 24.1° (atmospheric depth 664 gcm^{-2}) into account for generally observed shower events. The median zenith angles are 27.2° and 22.8° (681 gcm^{-2} and 657 gcm^{-2}) for the showers arriving from the inner and outer Galactic plane, respectively. Thus, the energy decline rate in gamma-initiated showers is somewhat reduced for the IG plane and magnified a little for the OG plane. On the other hand, the spectral index of the diffuse gamma rays is probably smaller than the 2.7 of the galactic cosmic rays at energies around 10 TeV. This produces an opposite offset of the observed gamma-ray energy. which shifts to a higher value, depending on the spectral index. If the gamma-ray spectral index is 2.4, as assumed in the derivation of the intensity upper limit in Table 2, gamma-ray energy goes up about 10% or more. The effects just described act to offset each other. Thus we use the observed energies, 3 TeV for the Tibet-III and 10 TeV for the Tibet-II, for the primary energies determined for the generally observed air showers at Yangbajing site.

Second, the sky regions searched for Galactic diffuse gamma rays have a shape like a convex lens along the Galactic plane as shown in Fig. 2. Such a lens shaped region is inevitable in our method, employing the warped belts along the Galactic plane in equatorial coordinates. The maximum thickness of the lens is 3.6° or 8.9°, but the simple mean of the range used is 3.5° or 8.7° for IG and 2.7° or 6.8° for OG in the 4° bin and 10° bin analyses, respectively. Taking the number density of events into account, the weighted mean thickness becomes 3.5° or 8.7° for IG and 2.9° or 7.2° for OG, respectively. As already described, the data in the two 2° bin belts has been excluded from the off-plane region for OG in order to minimize the influence of the Crab Nebula. Other strong gamma-ray sources, Geminga ($l = 195.03^\circ, b = 4.83^\circ$) and IC443 ($l = 188.83^\circ, b = 3.07^\circ$) are involved in the on-plane region of the OG plane in the 10° bin analysis. No TeV gamma-ray signal has, however, been obtained from these candidate sources by any surface air shower arrays or Cherenkov telescopes. Therefore, no correction for the influence of these candidates is necessary.

Third, according to the EGRET data Hunter et al. 1997 with $|b| \leq 2^\circ$, gamma-ray intensity shows a decline in the galactic longitude region from $l = 25^\circ$ to 65° in IG for every energy ranges, 30-100 MeV, 100-300 MeV, 300-1000 MeV and above 1000 MeV. This tendency is also seen in SAS-2 and COS-B data (see Bertsch et al. 1993). The intensity shows a rather flat top in the central range, $330^\circ \leq l \leq 25^\circ$. In our analysis, the inner Galactic region is located just at this region of declining intensity. The Whipple LeBohec et al. 2000 and HEGRA Aharonian et al. 2001 data also lie partially in this region, at around $l = 40^\circ$. If the intensity decline around 1 GeV is caused by the density distribution of ISPF, it is expected that the gamma-ray intensity shows similar behavior in the TeV region. We should compare the experimental data with the reduced intensity of about 80 % of the theoretical curves, which have been calculated for the central flat top region. This is the reason that the experimental data are not sufficient to rule out the inverse Compton model with a source spectral index of 2.0.

Theoretical calculations give an indication that, if the source electron spectral index in the 10 GeV to 10 TeV energy region is smaller than 2.4, the diffuse gamma rays in the TeV region are mainly generated by IC scattering. In that case, it is essential to fix the diffuse gamma-ray intensity to determine the source electron spectrum in the Galactic plane. This can suggest the strength of shock acceleration, and clarifies the electron propagation process in the Galactic disc through a comparison with the direct observation of local electrons, and also gives an estimate of average magnetic field in the source region by examining the consistency with the radio synchrotron intensity.

The extension of the Tibet-III array is expected to be completed by the end of 2002; its effective inner area will become about 1.5 times larger than at present, and 1.15 times larger than the Tibet-II inner area. If the new Tibet-III array continues for running three years without long suspension, statistics will increase to 4-5 times the present data at both 3 TeV and 10 TeV. The resulting statistical reduction in the upper limits, by a factor of 2 or more, will be more closely comparable with theoretical models, and can also give a significant upper limit at even higher energies, e.g., at 20 TeV, where the upper limit is relatively more sensitive to the acceleration energy cutoff in the IC model.

This work is supported in part by Grants-in-Aid for Scientific Research on Priority Areas from the Ministry of Education, Culture, Sports, Science and Technology in Japan and from the Committee of the Natural Science Foundation and the Academy of Sciences in China.

REFERENCES

Aharonian, F.A., & Atoyan, A.M. 2001, A&A, 362, 937

Aharonian, F.A. et al. 2001, A&A, 375, 1008

Amenomori, M. et al. 1992, Phys. Rev. Letters, 69, 2468

———-. 1993, Phys. Rev. D, 47, 2675

———-. 1995, Proc. 24th Int. Cosmic Ray Conf. (Rome), 3, 528

———-. 1996, ApJ, 464, 954

———-. 1997, Proc. 25th Int. Cosmic Ray Conf. (Durban), 3, 117

———-. 2001, Proc. 27th Int. Cosmic Ray Conf. (Hamburg), 2, 573

Apanasenko, A.V. et al. 2001, Astropart. Phys., 16, 13

Barwick, S.W. et al. 1998, ApJ, 498, 779

Berezhko, E.G., & Völk, H.J. 2000, ApJ, 540, 923

Berezinsky, V.S., Gaisser, T.K., Halzen, F., & Stanev, T. 1993, Astropart. Phys., 1, 281

Bertsch, D.L. et al. 1993, ApJ, 416, 587

Bloemen, J.B.G.M., Blits, L., & Hermsen, W. 1984, ApJ, 27 9, 136

Bloemen, J.B.G.M. 1985, A&A, 145, 391

Borione, A. et al. 1998, ApJ, 493, 175

Chi, X. et al. 1989, J. Phys. G, 15, 1495

Dermer, C.D. 1986, A&A, 157, 223

Feenberg, E., & Primakoff, H. 1948, Phys. Rev., 73, 449

Fichtel, C.E. & Kniffen, D.A. 1984, A&A, 134, 13

Fichtel, C. et al. 1972, ApJ, 177, 341

———-. 1975, ApJ, 198, 163

Ginzburg, V.L., & Syrovatskii, S.I. 1964, The O rigin of Cosmic Rays (Oxford: Pergamon Press)

Green, D.A. 1995, A Catalogue of Galactic SNR (Cambridge: Mullard RAO)

Hartman, R. et al. 1979, ApJ, 230, 597

Hayakawa, S. 1952, Prog. Theor. Phys. 8, 571

Helene, O. 1983, Nucl. Instr. & Methods, 212, 319

Hunter, S.D. et al. 1997, ApJ, 416, 587

Ingelman, G., & Thunman, M. 1996, preprint TSL/ISV-96-0136

Kasahara, K. & Torii, S. 1991, Comput. Phys. Commun., 64, 109

Kraushaar, W. et al. 1972, ApJ, 177, 341

LeBohec, S. et al. 2000, ApJ, 539, 209

Mathis, J.S., Mezger, P.G., & Panagia, N. 1983, A&A, 128, 212

Mayer-Hasselwander, H. et al. 1980, Ann. NY Acad. of Sci. No. 336, Ninth Texas Symposium on Relativistic Astrophysics (Munich), 211

———-. 1982, A&A, 105, 164

Mori, S. 1997, ApJ, 478, 225

Morrison, P. 1958, Nuovo Cimento, 6, 858

Pohl, M., & Esposito, J.A. 1998, ApJ, 507, 327

Porter, T.A., & Protheroe, R.J. 1997, J. Phys. G, 23, 1765

Protheroe, R.J. 1984, Astron. Express, 1, 33

Protheroe, R.J., & Wolfendale, A.W. 1980, A&A, 92, 175

Schlickeiser, R. 1979, ApJ, 233, 294

Stecker, F.W. 1988, Cosmic Gamma Rays, Neutrinos and Related Astrophysics, ed. M.M. Shapiro & J.P. Wefel (Dordrecht: Reidel) 85

Strong, A.W., Moskalenko, I.V., & Reimer, O. 2000, ApJ, 537, 763

Tateyama, N., & Nishimura, J. 2001, Proc. 27th Int. Cosmic Ray Conf. (Hamburg), 6, 2343; in preparation

Torii, S. et al. 2001, ApJ, 559, 973

Webber, W.R. 1999, Proc. 26th Int. Cosmic Ray Conf. (Salt Lake City), 4, 97

This preprint was prepared with the AAS LaTeX macros v4.0.

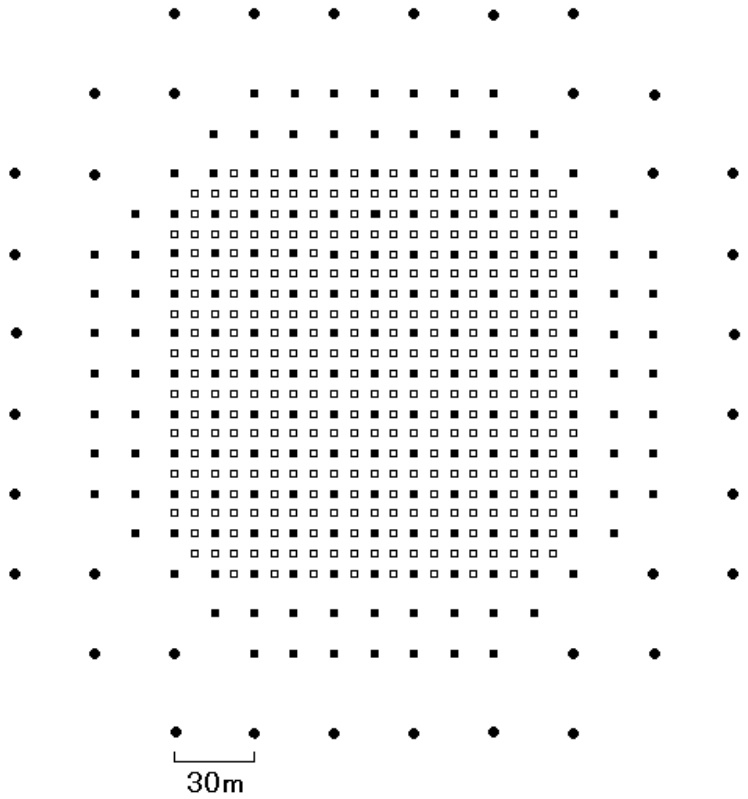

Fig. 1.— Array map of the Tibet-II and Tibet-III at Yangbajing. Filled squares are detectors in the Tibet-II (1995-1999) and open ones are added detectors to construct the Tibet-III (1999-2002). Filled circles are density detectors equipped with a wide dynamic range phototube.

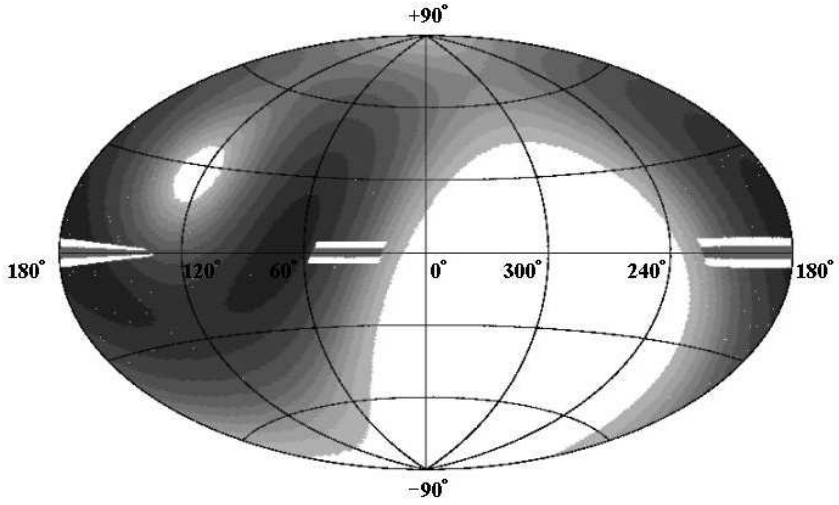

Fig. 2.— Tibet-III exposure map in the galactic coordinates for showers with zenith angles $\theta \leq 50°$. The event density increases from light gray to dark gray. Boundaries of searched sky region for diffuse gamma rays from the Galactic plane are indicated by narrow gray ($|b| \leq 2°$) and white plus gray ($|b| \leq 5°$) along the Galactic plane.

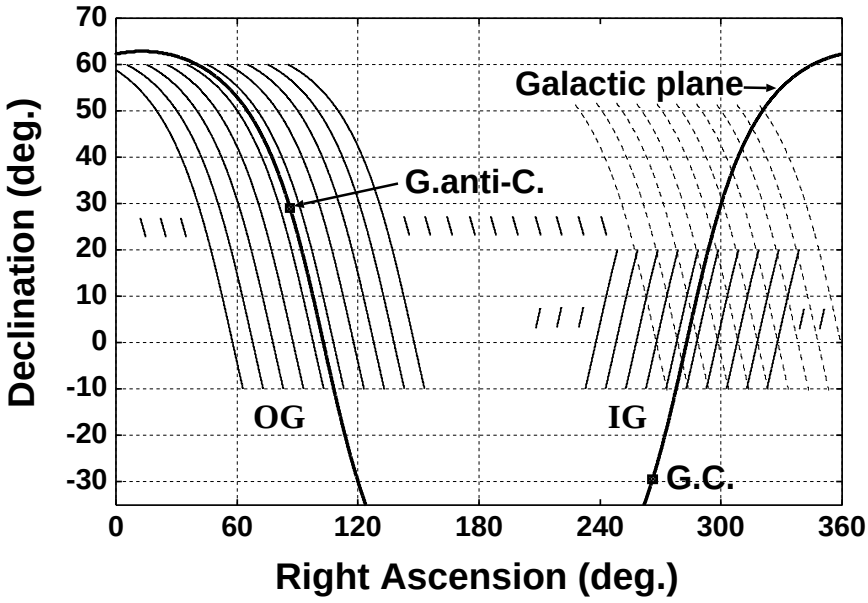

Fig. 3.— Warped belts of 10° width in the right ascension along the Galactic plane for IG near the Galactic center and OG including the Galactic anticenter.

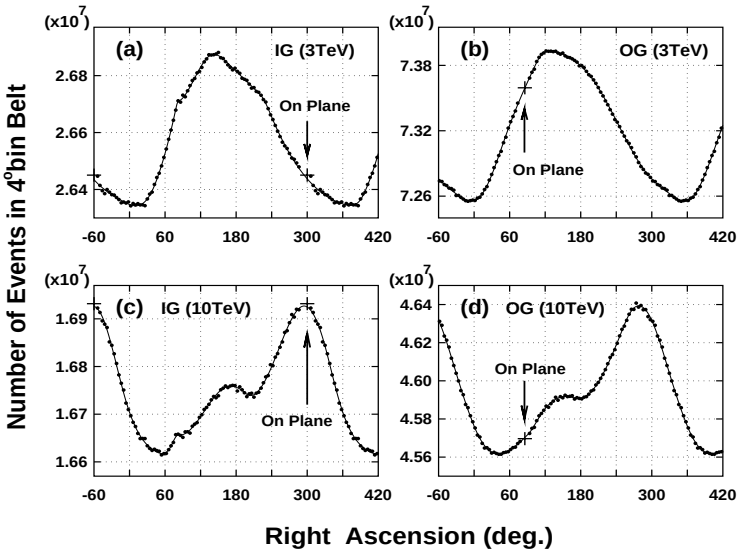

Fig. 4.— Distributions of number of events in 4° bin warped belts for (a) IG and (b) OG in Tibet-III data at 3 TeV and (c) IG and (d) OG in Tibet-II data at 10 TeV. Abscissa represents the right ascension of each belt at the declination 30°. Solid lines are curves fitted to the experimental data. In each subfigure, the on-plane data point is shown by a large + for the 4° bin analysis.

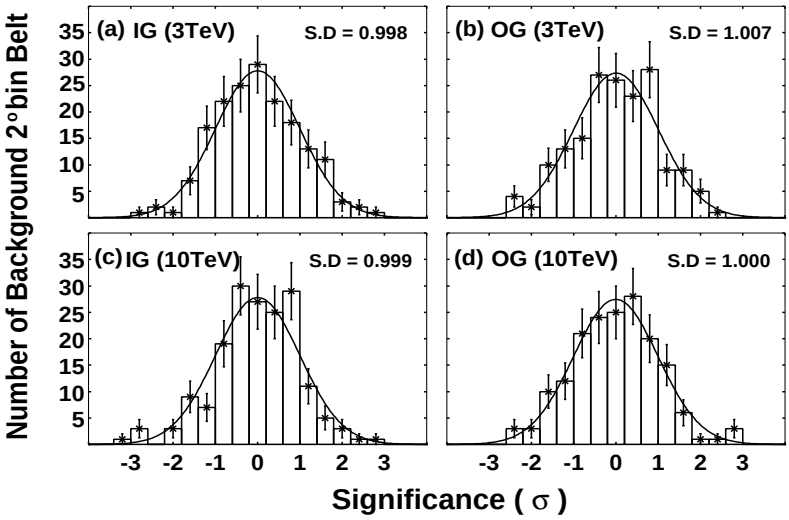

Fig. 5.— Deviation distributions of 2° bin off-plane data from the fitted curves for (a) IG and (b) OG for the Tibet-III data at 3 TeV, and (c) IG and (d) OG for the Tibet-II data at 10 TeV in the 4° bin analysis. For IG, the data in the central 12° are omitted from the off-plane data. For OG, the data in the range $-10^\circ \leq l \leq 6^\circ$ are also excluded to minimize the Crab's influence in the 4° bin analysis. Solid curves are best-fit Gaussians with standard deviation designated in each subfigure.

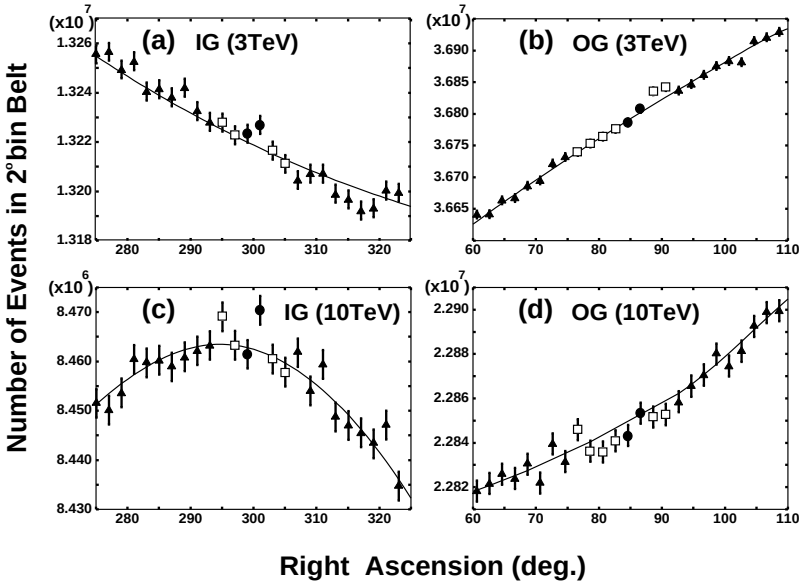

Fig. 6.— Distributions of the number of events in the right ascension range of 50°. Subfigures (a), (b), (c) and (d) correspond to those in Fig. 4. Abscissas are the same in Fig. 4. On-plane data are shown by filled circles, off-plane data by filled triangles, and open squares indicate data omitted from the background estimation, as described in the text. The fitted solid curves in each subfigure are used for estimation of the number of on-plane background events B. $E - B$ is the excess number of events over the solid curves in the on-plane belts.

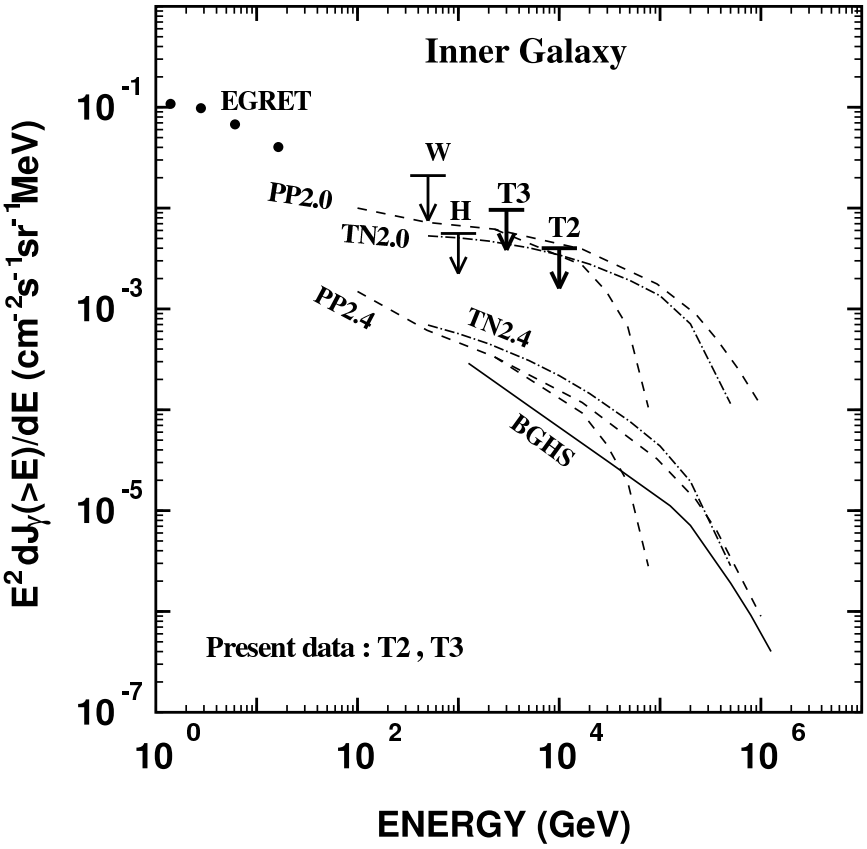

Fig. 7.— Diffuse gamma rays from the inner Galaxy (IG). Present data are labeled by T2 and T3 as 99% CL upper limits, assuming a gamma-ray spectral index 2.4. W and H indicate the Whipple's 99.9% CL LeBohec et al. 2000 and HEGRA's 99% CL Aharonian et al. 2001 upper limits with IACT. Theoretical curves are labeled by initials of the authors names. BGHS represents $\pi^\circ \rightarrow 2\gamma$ by Berezinsky et al. (1993). PP and TN are given by Porter & Protheroe (1996) and Tateyama & Nishimura (2001) for the inverse Compton. The numerals 2.0 or 2.4 following PP and TN indicate the electron source differential spectral indices.

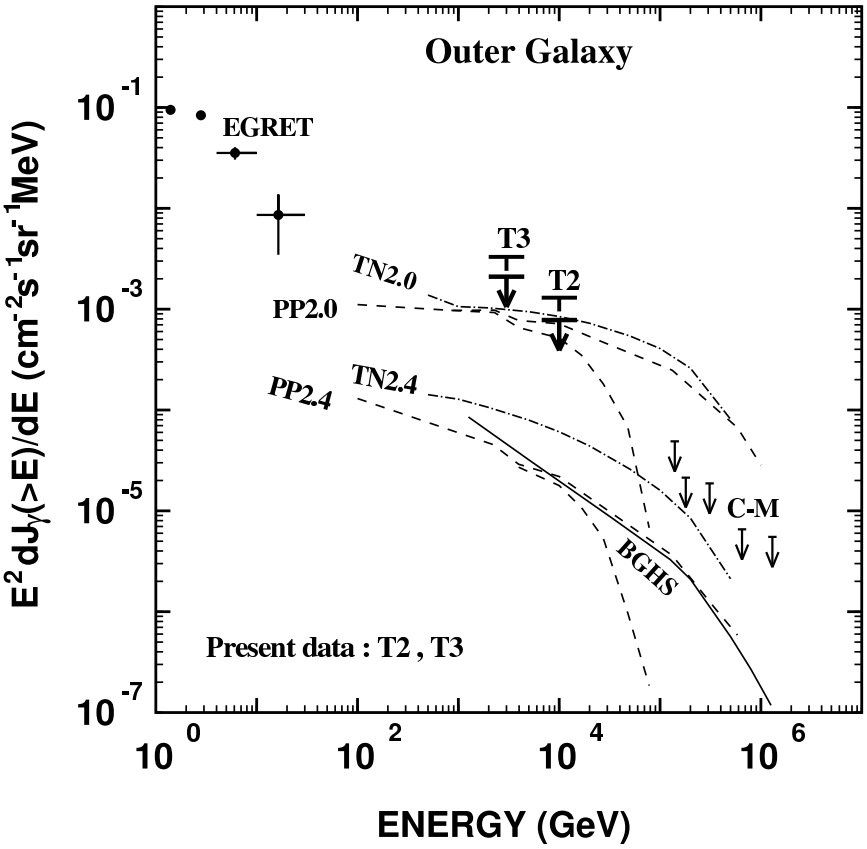

Fig. 8.— Diffuse gamma rays from the outer Galaxy (OG). Present data are labeled by T2 and T3 as 99% CL (upper bars) and 90% CL (lower bars) upper limits, assuming the same spectral index 2.4. The latter are compared with CASA-MIA 90% CL upper limits (labeled by C-M), based on muon-poor air shower data Borione et al. 1998. Theoretical curves and their labels are the same as in Fig. 7.